IOP Conf. Series: Journal of Physics: Conf. Series **843** (2017) 012027 doi:10.1088/1742-6596/843/1/012027

Fatigue in a heat treatable high silicon containing aluminium alloy

J.A. González[1], J. Talamantes-Silva[1], S. Valtierra[1] and Rafael Colás[2]

[1] Nemak México, S.A., Libramiento Arco Vial Km. 3.8, 66000 García, N.L., México.
[2] Facultad de Ingeniería Mecánica y Eléctrica, Universidad Autónoma de Nuevo León, 66455 San Nicolás, N.L., México.
Corresponding author: rafael.colas@uanl.edu.mx

Abstract. The use of cast aluminium alloys in automobiles contributes to reductions in weight and fuel consumption without impairing the safety for the occupants or the performance of the car. Most of the alloys used are heat treatable hypoeutectic Al-Si alloys, which have the drawback of exhibiting low wear resistance. So industry relies in wear resistant alloys, such as grey iron, for the liners of the combustion chambers in engine blocks, which increase the weight of the engine. Therefore, it is of interest to cast high silicon containing alloys into engine components that are able to resist wear while maintaining the mechanical properties required by the components. This work presents the result of the work carried out in a high silicon containing heat treatable aluminium alloy as it is subjected to high cycle fatigue. The alloy was prepared and cast in ingots designed to promote one dimensional solidification gradient to obtain samples to study the high cycle fatigue. The material was machined into hour-glass specimens that were tested at room temperature in a servohydraulic machine under load control following the stair case method. The results show that the resistance to fatigue depends on the microstructure of the sample, as the fatigue cracks originate in pores close to the surface of the sample and propagate through the eutectic aggregate. The results from this work are compared with those from previously obtained with hypoeutectic alloys.

1. Introduction

The engine block in automobiles converts chemical into mechanical energy by burning fuel within the combustion chambers. Most of the energy produced by the explosion of the air-fuel mixture is converted into heat, which has to be extracted through the walls of the chambers to the proper block and to the refrigerating fluids. Heat extraction has to be efficient otherwise the engine block may be subjected to excessive thermal loads that will modify the mechanical properties of the alloy from which the block is made, leading to its catastrophic failure [1,2]. Engine blocks in automobiles have been migrating from cast iron to aluminium alloys [3,4] to reduce their weight, improve fuel consumption and comply with environmental regulations imposed by governments in different countries. Unfortunately, conventional aluminium alloys do not exhibit the resisting capabilities required for sustaining the wear caused by the reciprocating movement of the pistons, so most engine blocks are manufactured with sleeves or liners made from wear resistant alloys, which will result in the increase of around 6 kg in a V8 engine when grey iron liners are used [2,5].

Hypereutectic Al-Si alloys are used in applications in which resistance to wear is adamant, due to the presence of primary silicon crystals, nevertheless these crystals pose a machinability problem for engine plants, and may not be able to comply with the rigorous static and dynamic mechanical properties demanded by the use in engine blocks [5-10].

The defects that are present in cast aluminium alloys affect their resistance to fatigue; the flaws that exert the higher influence are pores, either due to shrinkage or gas evolution, hard components of eutectic aggregates, intermetallic inclusions and precipitated particles, as cracks nucleate on the defects and grow following paths in which other smaller faults are concentrated [11-22]. The distribution and size of such defects are modified by augmenting the rate at which the casting solidifies; as smaller sizes and finer distribution are obtained by the increased nucleation and reduction in the time available for growing [3,4,23,24]. The most common method to assess the degree of microstructural refining is by means of the secondary dendrite arm spacing, DAS, which is related to the heat transfer rate occurring during solidification [4,23,24]. As fatigue cracks nucleate and grow from existing defects, it is of critical importance to determine the type of defects that exert the higher influence [11-22].

The aim of this work is to present the results of a series of studies carried out to evaluate the fatigue resistance of a cast aluminium alloy containing high amounts of silicon, as it is intended for the manufacture of automotive components. The study was conducted on heat treated samples that had different degrees of microstructural refining as they were obtained from ingots designed for this purpose.

2. Experimental procedure

The alloy (13.5 Si, 2.9 Cu, 1.4 Ni, 0.3 Mg, 0.15 Fe, 0.12 Ti, 0.07 Sr, wt.%) was prepared in a gas fired furnace of 250 kg of capacity. The liquid was kept at 760°C as it was degassed with nitrogen before adding titanium and strontium to refine the grain size and modify the eutectic aggregate; the melt was poured into sand moulds that contained a grey iron chilling plate at their bottom to promote directional solidification, Fig. 1a. The ingots were cut to obtain prismatic bars that were heat treated to obtain a T7 condition. Solution was carried out at 495°C for 5 h, followed by cooling in water at 90°C and aged at 240°C for 5 h. Three different levels of microstructural refining were considered. The bars that correspond to Level I are 1 to 4, those of Level II are 7 to 13 and for Level III are 18 to 25, Fig. 1b.

The material was machined into cylindrical bars of 15.0 ± 0.02 mm to produce hour-glass shape specimens that had a reduced diameter of 6.0 ± 0.05 mm at their centre, following a radius of curvature of 48.0 ± 0.25 mm. Tensile test were carried out the ASTM standards B-557 [25] and E-8 [26] in specimens of 12.7 mm in diameter by 62.7 mm in gauge length; the values of the yield (σ_y) and tensile (σ_u) strength, and total elongation (Δl) were recorded.

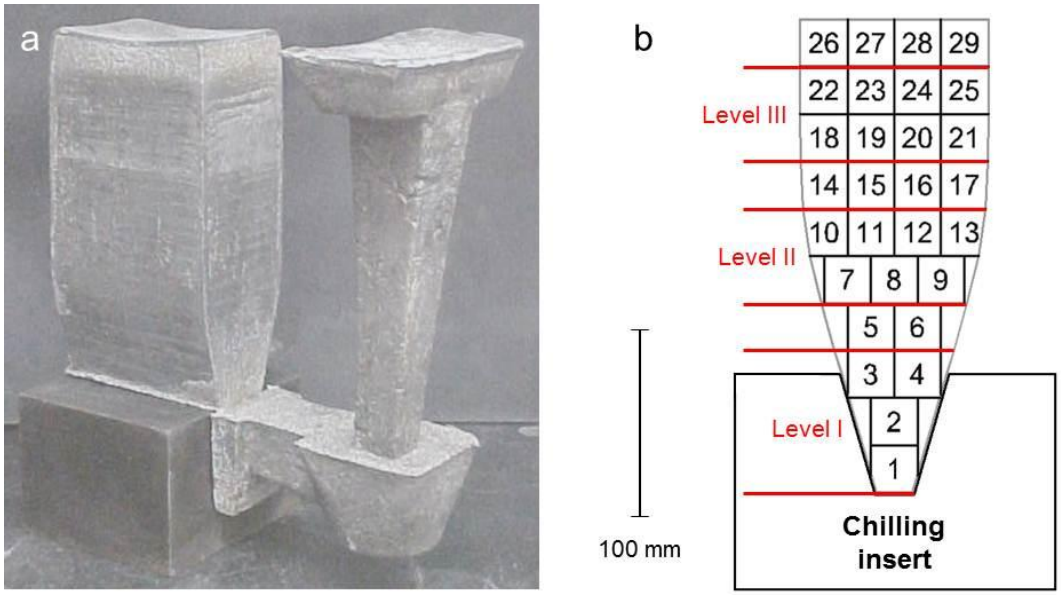

Figure 1. Photograph of one of the ingots into which the melt was cast, a; identification of the bars that were sectioned and treated to obtain the three levels of microstructural refining, b.

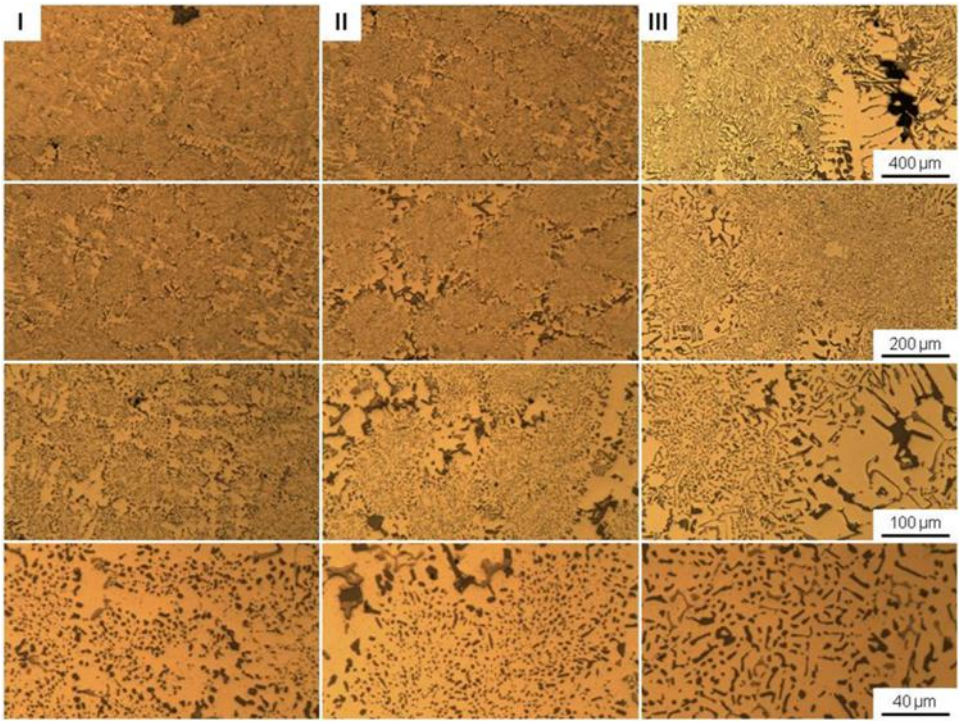

Figure 2. Microstructures of the samples at different magnification at the three different levels.

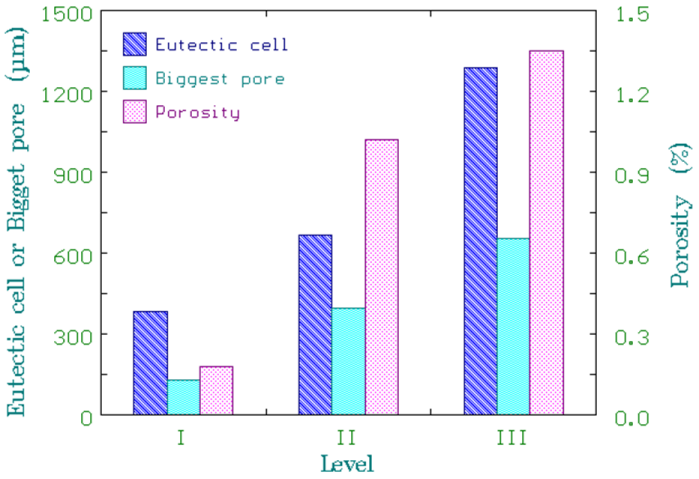

Figure 3. Sizes of the eutectic cell and biggest pore, and that of the porosity detected in the samples.

Fatigue tests were fully reversible (R = -1) and were conducted at 70 Hz at room temperature in a ±25 kN servohydraulic testing machine; chucks commonly in lathes for turning operations were used as grips to avoid the mechanical inertia caused by the hydraulic grips normally use in fatigue tests. These chucks had the limitation of not being able to sustain loads higher than 4.5 kN. Fatigue testing followed a reduced staircase schedule [27]; the specimens were tested up to failure or until a number of 10^7 cycles was achieved; the reversible stress was computed from the original cross-section of the specimen. The trials started at values of stress that did not surpassed the yield point and these values were then reduced by 10 MPa in the following test upon failure; this procedure was modified to reduce or increase the stress in 5 MPa steps once the sample resisted the 10^7 cycles. The samples that resisted 10^7 cycles were then subjected to fatigue at a stress level 10% higher to promote their failure and measure the size of the defect on which the crack was nucleated. All results are referred to the reversing cyclic stress or $\Delta\sigma/2$.

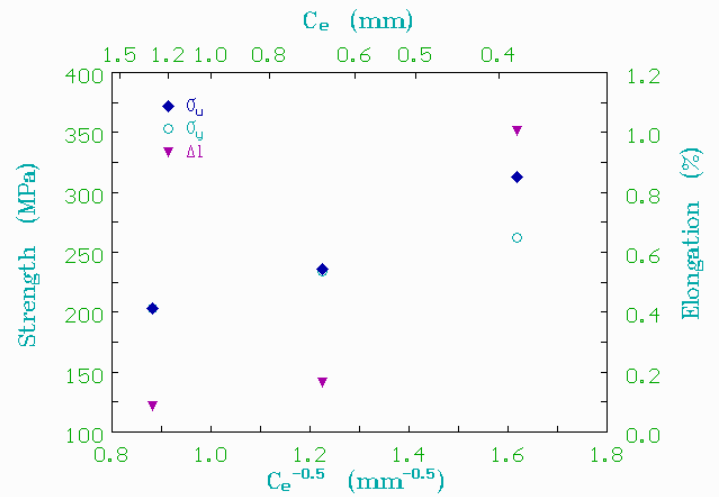

Figure 4. Dependence of the mechanical properties in tension as a function of the square root of the dendritic cell

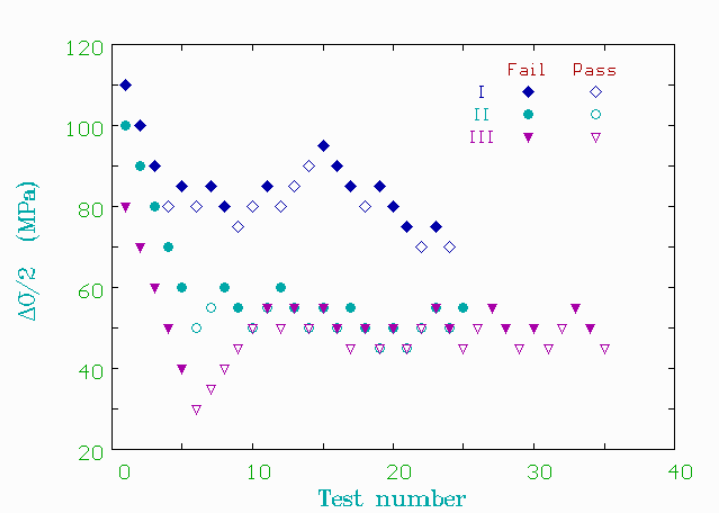

Figure 5. Staircases conducted on samples from the three different levels.

Failure and metallographic analyses were conducted on fractured specimens by scanning electron microscopy (SEM) and optical microscopy (OM). The size and type of defect that originated the failure by fatigue, as well as the distance and area of propagation of the crack was recorded by observation by SEM. This information was used to calculate design parameters that included fracture toughness (K_{IC}), maximum stress intensity factor (ΔK_{max}), as well as relationship between these parameters and the total number of cycles and maximum stress amplitude that a particular specimen was able to endure [28-30].

3. Results

The microstructures of the samples heat treated to the T7 condition are shown in Fig. 2, in which some dendrites can be distinguished, although the alloy does not solidify following the traditional dendritic growth characteristic of hypoeutectic Al-Si alloys. The dominant microstructural parameter in this alloy is the eutectic cell (C_e), which is affected by the solidification rate. Fig. 3 shows the values that this parameter, as well as the size of the biggest pore and the amount of porosity encountered at the different levels being considered. It was found that the mechanical properties depend on the inverse of the square root of the dendritic cell, Fig. 4. Table 1 shows the values of the microstructural features and those of the mechanical properties recorded in tensile tests and deduced from the fatigue tests.

Table 1. Properties and characteristics of the material at different levels.

Level	σ_y (MPa)	σ_u (MPa)	Δl (%)	σ_f (MPa)	K_{IC} (MPa·m$^{0.5}$)	C_e (µm)	BP* (µm)	Porosity (%)
I	262	313	1.01	81.4	32.7	387	128	0.18
II	234	236	0.17	52.5	29.2	635	396	1.02
III	203	203	0.09	48.2	22.3	1250	656	1.35

* Biggest pore

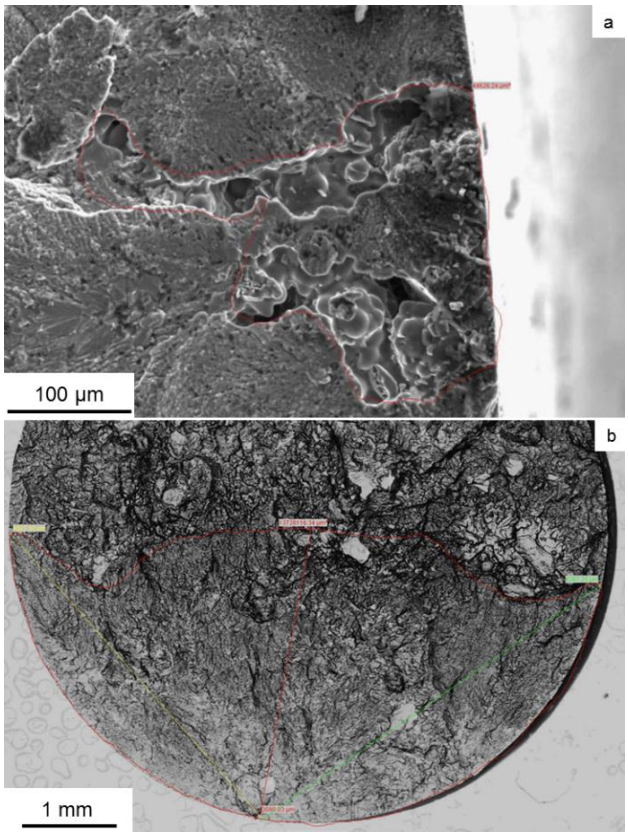

Figure 6. Pore that originated the crack, a, and distance and surface that the crack propagated in fatigue, b, before causing the failure of the sample.

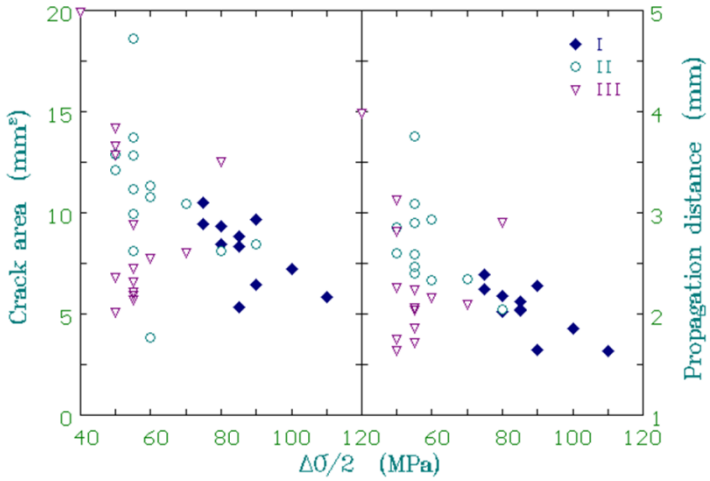

Figure 7. Area and distance that the crack propagated as a function of the nominal applied stress.

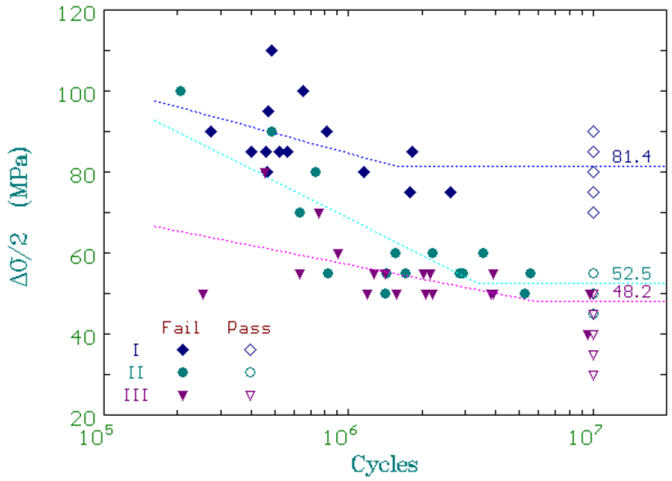

Figure 8. S-N plots for the three different levels.

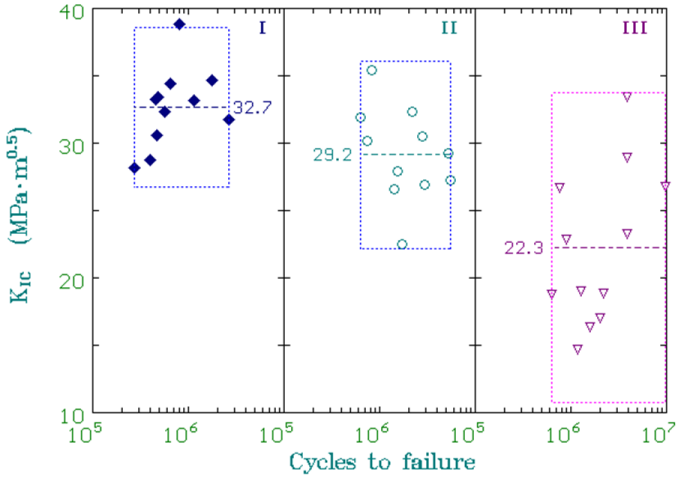

Figure 9. K_{IC} for the specimens that failed before reaching 10^7 cycles.

Fig. 5 shows the staircase schedules for the tests conducted, the specimens that failed before reaching the 10^7 cycles, or that resisted this number are identified by either full or empty symbols; the stress applied to a given specimen was reduced when the previous one failed, or increased, when the full number of cycles was achieved. The samples that survived the 10^7 cycles were then fatigued at a stress level 10% higher to promote their failure and measure the size of the defect on which the crack was nucleated.

The fracture surface of the samples was observed by SEM to detect the origin of the failure and measure its size and the area and distance that the fracture was able to propagate in fatigue before causing the failure of the sample. An example of the measurements carried out on every sample is shown in Fig. 6. It was found that the distance and area that the cracks propagated are related to the cycles to failure and to the nominal stress applied, Fig. 7 shows the relationship between these parameters and the nominal applied stress.

The fatigue stress limit (σ_f) was computed following the procedure for evaluating castings [27]:

$$\sigma_f = \sigma_o + \delta\sigma\left(\frac{\sum i n_i}{N} + \frac{\delta\sigma}{2}\right) \quad (1)$$

where σ_o corresponds to the lowest value of stress that was tested, $\delta\sigma$ is the step size in the final part of the staircase schedule (5 MPa), n_i is the number of pieces that resisted 10^7 cycles at each i stress interval, N is the total number of samples that resisted all the cycles.

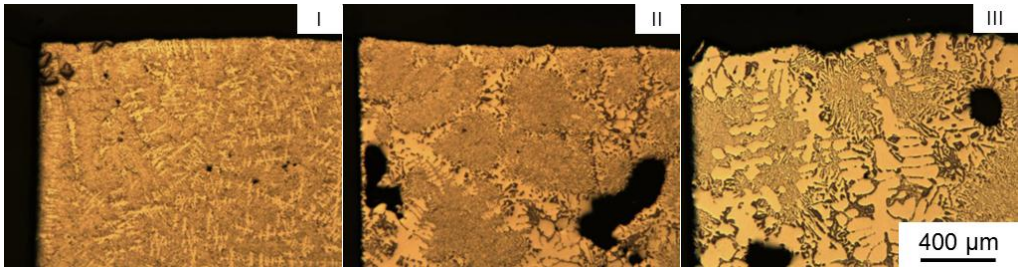

Figure 10. Metallographic observation of samples fatigued at different levels.

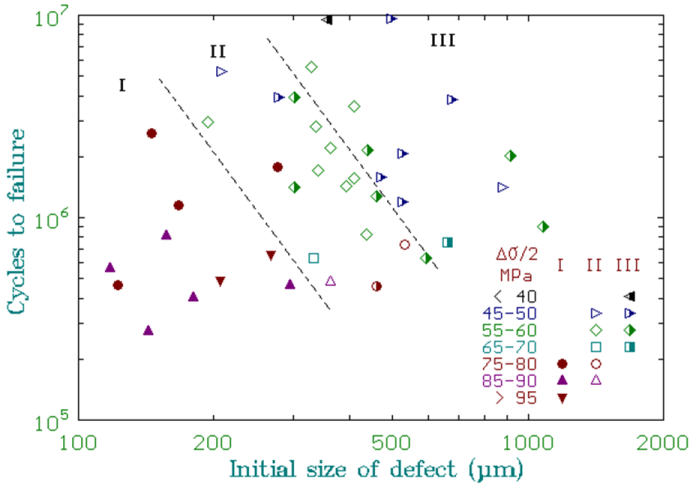

Figure 11. Cycles to failure as a function of the size of defect that originated the crack.

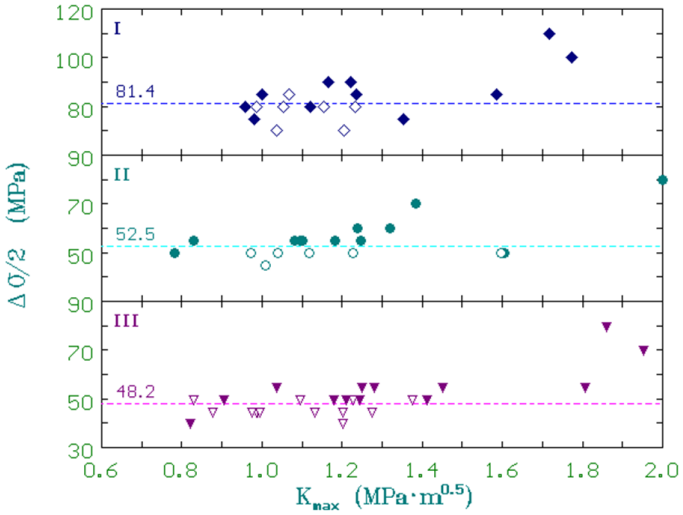

Figure 12. ΔK_{max} for the material tested. The specimens that resisted 10^7 cycles were then fatigued at a 10% stress to obtain the size of the pore that originated the crack.

4. Discussion

The S-N curves of the material are shown in Fig. 8. The fatigue limits shown in the figure and in Table 1 were calculated from the reduced staircases. The values of the mechanical properties and for the limit of fatigue for the samples from level I are comparable to those reported for a hypoeutectic alloy used in the manufacture of automotive blocks [21,22]. The toughness of the material obtained at different levels, K_{IC}, is calculated by [30]:

$$K_{IC} = K_T \alpha \sigma_{mx} \sqrt{\pi a_c} \quad (2)$$

where α is a parameter that takes the value of 1.12 and represents the edge factor, K_T represents the concentration of stress due to the geometry of the defects and takes the value of 3 as it is considered that the crack follows a circular shape, σ_{mx} is the stress that promoted the fracture and a_c corresponds to the size of the crack, which corresponds to the propagated distance in Fig. 6. Fig. 9 shows the relationship between the value of K_{IC} and the number of cycles to fracture; the average values of K_{IC} for the specimens that did not resist the full 10^7 cycles are shown in Table 1.

Figure 10 shows a series of samples that were prepared for their metallographic observation after failing the fatigue test. The crack originated in all cases in a pore located at the upper left corner in each sample. The presence of massive silicon particles can be appreciated close to the origin of the fracture in the sample from level I which may be indicative that the pores are the predominant defect in which the cracks are formed. Such observation is confirmed in Fig. 11 in which the number of cycles to failure is plotted as a function of the size of the defect on which the crack initiated; it is worth noticing how the data can be segregated in regions for each level, as the size of the pores in level III samples are bigger than in the other two conditions. It is also clear from this figure that the samples from level I fail at a higher reversing stress.

Murakami et al. [28,29] showed that the maximum value for the stress intensity factor (ΔK_{max}) depends on the area of the defect and its location, rather than on its shape; with this assumption, the threshold for R = -1 can be calculated by:

$$\Delta K_{\max} = \beta \Delta\sigma \sqrt{\pi \sqrt{A_d}} \tag{3}$$

where β is a parameter that takes the value of 0.65 for cracks originated at pores close to the surface and 0.50 for cracks that originated in internal pores. The area of the defect that originated the crack, A_d, and its location was evaluated by **SEM**. For fully reversed fatigue cycling (R = -1) $\Delta\sigma = \sigma_{mx} - \sigma_{mn}$; since $\sigma_{mn} = -\sigma_{mx}$, then $\Delta\sigma = 2\sigma_{mx}$. The values for ΔK_{max} computed from the fractographic analyses and the experimental data are shown in Fig. 12. The full symbols represent samples that failed before the 10^7 cycles were achieved, the open symbols correspond to samples that resisted such level of cycles, but were broken at a 10% higher stress. A problem that was encountered in this type of alloy is the overlapping of the values corresponding for ΔK_{max} for samples that resisted the test and those that did not, contrary that is found in hypoeutectic alloys [21,22]. A reason for this behaviour may be the way in which the crack propagates. Low silicon containing alloys are made of a dendritic aluminium matrix with the eutectic aggregate around them; in contrary, the high silicon containing alloy is made of eutectic cells with aluminium dendrites or primary silicon particles, Figs. 2 and 10. In the hypoeutectic case, the aluminium dendrites are ductile enough and are able to resist the propagation of the crack, whereas in the present case, the crack is able to propagate rapidly following the silicon particles that form part of the eutectic cell, as can be seen by observing the contour of the cracks shown in Fig. 13.

5. Conclusions

An aluminium alloy containing high levels of silicon and other elements was tested to study its behaviour a high cycle fatigue. The alloy was cast in ingots designed to produce a solidification gradient to vary the microstructure of the samples intended to study.

It was found that the mechanical properties and the limit of fatigue depended on the degree of microstructural refining, as the cracks that cause the failure in fatigue are nucleated in pores generated during casting. The mechanical properties of the alloy were found to be comparable to those characteristic of a hypoeutectic alloy used in the manufacture of engine blocks.

The toughness of the material was calculated by means of the size of the defect that originated the crack and that of the area that the crack propagated in fatigue before failure. It was not possible to assess the stress intensity factor as the crack propagates following the boundaries of the eutectic cells.

6. Acknowledgements

The authors acknowledge the support provided by the National Council for Science and Technology (CONACYT), Mexico.

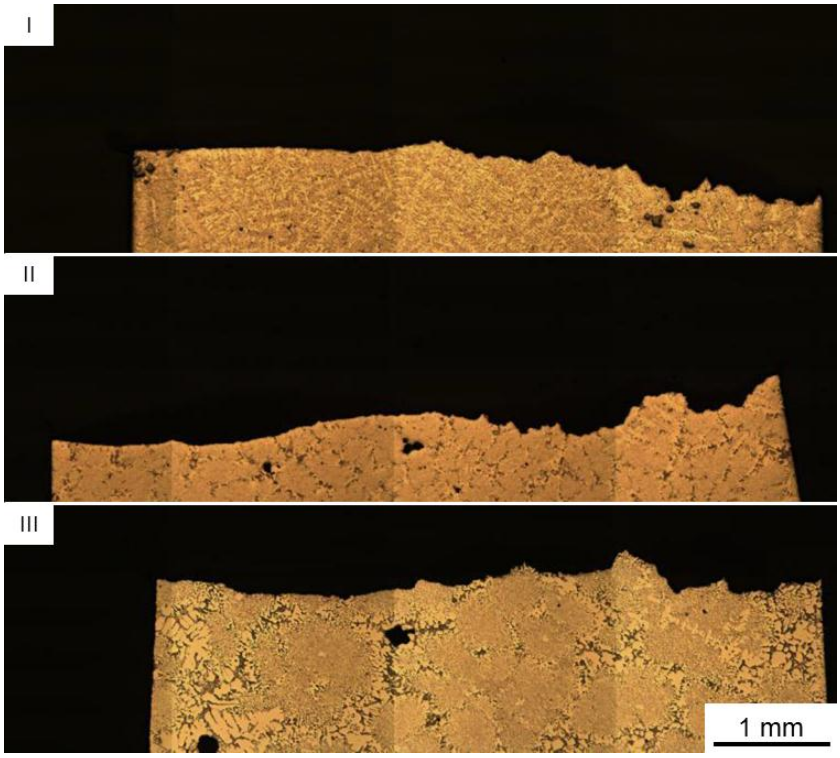

Figure 13. Contour of cracks that follow the eutectic cells and were observed in samples from different levels.

References

[1] Heywood, J.B., Internal Combustion Engine Fundamentals, McGraw-Hill, New York, 1989.
[2] Hoag, K., Vehicular engine design, Springer Science & Business Media, Wien, New York, 2007.
[3] Campbell, J., Castings, 2nd Ed., Butterworth-Heinemann, Oxford, 2003.
[4] Colás, R., Velasco, E. and Valtierra, S., Castings, Handbook of Aluminum, Vol. 1: Physical Metallurgy and Processes, G.E. Totten and D.S. MacKenzie (eds.), M. Dekker, New York, 2003, 591-641.
[5] Foss, J.E., Krug, P.L. and Kennedy, M., New aluminum alloys for cylinder liner applications, SAE Techn. Paper 2006-01-0983, SAE International, Warrendale, 2006.
[6] Tenekedjiev, N. and Gruzleski, J.E., 1990. Hypereutectic aluminium-silicon casting alloys-a review. *Cast Met.*, **3**, 96-105.
[7] Vijeesh, V. and Prabhu, K.N., 2014, Review of microstructure evolution in hypereutectic Al–Si alloys and its effect on wear properties. *Trans. Ind. Inst. Met*., **67**, 1-18.
[8] Donahue, R. and Fabiyi, P.A., 2000. Manufacturing feasibility of all-aluminum automotive engines via application of high silicon aluminum alloy (No. 2000-01-0061). SAE Technical Paper.
[9] Doty, H.W., General Motors Corporation, 2005. Aluminum alloy for engine blocks. U.S. Patent 6,921,512.
[10] Kasprzak, W., Sokolowski, J.H., Yamagata, H., Aniolek, M. and Kurita, H., 2011. Energy efficient heat treatment for linerless hypereutectic Al-Si engine blocks made using vacuum HPDC process. *J. Mat. Eng. Perf.*, **20**, 120-132.
[11] Surappa, M.K., Blank, E. and Jaquet, J.C., 1986, Effect of macro-porosity on the strength and ductility of cast Al-7Si-0.3Mg alloy, *Scr. Metall.*, **20**, 1281-1286.
[12] Skallerud, B., Iveland ,T. and Harkegard, G., 1993, Fatigue life assessment of aluminum alloys with casting defects, *Eng. Fract. Mech.*, **44**, 857-874.

[13] Stanzl-Tschegg, S.E., Mayer, H.R., Tschegg, E.K. and Beste, A., 1993, In-service loading of AlSi11 aluminium cast alloy in the very high cycle regime, *Int. J. Fat*., **15**, 311-316.
[14] Major, J.F., 1998, Porosity control and fatigue behavior in A356-T61 aluminum alloy, *Trans. AFS*, **105**, 901-906.
[15] Seniw, M.E., Conley, J.G. and Fine, M.E., 2000, The effect of microscopic inclusion locations and silicon segregation on fatigue lifetimes of aluminum alloy A356 castings, *Mat. Sc. Eng. A.*, **285**, 43-48.
[16] Gall, K., Yang, N., Horstemeyer, M., McDowell, D.L. and Fan, J., 2000, The influence of modified intermetallics and Si particles on fatigue crack paths in a cast A356 Al alloy, Fat. *Fract. Eng. Mat. Struct.*, **23**, 159-172.
[17] Chen, W., Zhang B. and Poirier, D.R., 2000, Effect of solidification cooling rate on the fatigue life of A356.2-T6 cast aluminium alloy, *Fat. Fract. Eng. Mat. Struct.*, **23**, 417-423.
[18] Boileau, J.M. and Allison, J.E., 2003, The effect of solidification time and heat treatment on the fatigue properties of a cast 319 aluminum alloy, *Metall. Mat. Trans. A*, **34A**, 1807-1820.
[19] Chan, K.S., Jones, P. and Wang, Q., 2003, Fatigue crack growth and fracture paths in sand cast B319 and A356 aluminum alloys, *Mat. Sc. Eng. A.*, **341**, 18-34.
[20] Wang, Q.G., Davidson, C.J., Griffith, J.R. and Crepeau, P.N., 2006, Oxide films, pores and fatigue lives of cast aluminum alloys, *Metall. Mat. Trans B*, **36B**, 887-895.
[21] González, R., Martínez, D.I., González, J.A., Talamantes, J., Valtierra, S. and Colás, R., 2011, Experimental investigation for fatigue strength of a cast aluminium alloy, *Int. J. Fat.*, **33**, 273-278.
[22] González, R., González, A., Talamantes-Silva, J., Valtierra, S., Mercado-Solís, R.D., Garza-Montes-de-Oca, N.F. and Colás, R., 2013, Fatigue of an aluminium cast alloy used in the manufacture of automotive engine blocks, *Int. J. Fat.*, **54**, 118-126.
[23] Jaquet, J.C. and Hotz, W., 1992, Quantitative description of the microstructures of aluminum foundry alloys, *Cast Met.*, **4**, 200-225.
[24] Biloni, H. and Boettinger, W.J., 1996, Solidification, Physical Metallurgy, 4th Ed., R.W. Cahn and P. Haasen (eds.), North Holland, Amsterdam, 669-842.
[25] ASTM International, 1994, ASTM B557M-94: Standard Test methods of tension testing wrought and cast aluminum and magnesium alloy products (metric), West Conshohocken.
[26] ASTM International, 1999, ASTM E8M-99: Standard Test methods for tension testing of metallic materials (metric), West Conshohocken.
[27] GM Engineering Standards, 2002, GMN7152: Specification and verification of tensile and fatigue properties in cast components, General Motors Corporation, Detroit.
[28] Murakami, Y. and Endo, M., 1994, Effect of defects, inclusions and inhomogeneities on fatigue strength, Int. J. Fatigue, 16, 163-181.
[29] Murakami Y. and Beretta, S., 1999, Small defects and inhomogeneities in fatigue strength: Experiments, models and statistical implications, Extremes, 2, 123-147.
[30] Stephens, R.I., Fatemi, A., Stephens, R.R. and Fuchs, H.O., 2001, Metal Fatigue in Engineering, 2nd Ed., John Wiley & Sons, Inc., NY.